PHYSICAL REVIEW B **87**, 174104 (2013)

# Shock-compressed graphite to diamond transformation on nanosecond time scales

J. M. Winey and Y. M. Gupta

*Institute for Shock Physics and Department of Physics, Washington State University, Pullman, Washington 99164-2816, USA*

(Received 22 January 2013; published 17 May 2013)

Numerical simulations of previous plane shock wave measurements on highly oriented pyrolytic graphite (HOPG), shocked to four peak stresses ranging from 27 to 50 GPa, are presented to address a long-standing question: When is the diamond phase formed in the shock-compressed graphite to diamond transition? A multiphase material description was developed to simulate measured wave profiles in shocked HOPG. Our results showed good agreement with the measured profiles for all four peak stresses and demonstrated the following: Transformation is completed in less than 10 ns, the density and stiffness of the high-pressure phase match that of cubic diamond, and the mechanical response of the diamond phase is nonlinear elastic.

DOI: 10.1103/PhysRevB.87.174104 PACS number(s): 64.70.K−, 46.15.−x, 62.20.−x, 62.50.Ef

## I. INTRODUCTION

Since the recovery of cubic diamond from shock-compressed graphite powders was first reported by DeCarli and Jamieson in 1961,[1] the shock-induced graphite to diamond phase transformation has been the subject of considerable scientific and technological interest.[2–22] A good understanding of this particular transition is important for gaining insight into shock-induced phase transformations,[2] study of meteorite impacts,[3,4] technological applications involving the synthesis of industrial diamonds,[5,6] and for linking the shock work to static high-pressure–high-temperature (HP-HT) studies.[7] Although gem quality diamonds can now be fabricated routinely using chemical vapor deposition (CVD) approaches,[23,24] a detailed understanding of the shock-induced graphite to diamond transformation remains an important scientific challenge.

Based on early experiments[8–16] on shocked graphite powders, several reconstructive transformation mechanisms were proposed.[13,14,16,17] However, the lack of time-resolved measurements left an important question unanswered: What is the time scale for the formation of the diamond phase when graphite is shock compressed?

Erskine and Nellis's efforts[18,19] to address this question, through time-resolved wave profile measurements on highly ordered pyrolytic graphite (HOPG) shocked in plate impact experiments to 27–50 GPa stresses, are noteworthy. These measurements—the first of their kind for shocked graphite—revealed a clean, two-wave structure, with a transformation stress of 20 GPa, that indicated a rapid (<10 ns) phase transformation. Due to the fast transformation rate and the low temperature estimated for shocked HOPG, the transformation mechanism was described as martensitic. However, based on a comparison of the measured second phase Hugoniot (or end states) for shocked HOPG with a diamond Hugoniot extrapolated from high stress (>100 GPa) data,[25] they inferred that the high-pressure phase was 5% less dense than the expected diamond phase.[19] This inference raises the question: What is the nature of the high-pressure phase when HOPG is shocked above the transition stress? Although additional attempts to analyze the measured wave profiles were made using different theoretical approaches and different material modeling assumptions,[20–22] none provided quantitative agreement with the experimental results.

Since the cubic diamond phase is obtained in recovery experiments on shocked graphite (nonplanar shock wave loading), the Erskine and Nellis[19] work raises additional questions: Is nonplanar loading required to achieve the cubic diamond phase, and/or is it the longer time scale in recovery experiments that permits the transformation to proceed to the cubic diamond phase?

The previous efforts for analyzing shocked HOPG[19–22] were hindered by a scarcity of information regarding the mechanical response of the high-pressure phase. In particular, the lack of experimental results for shock-compressed diamond at similar stresses makes it difficult to undertake detailed comparisons between the high-pressure phase results and the diamond results. This need was addressed recently;[26,27] high-quality wave profiles were measured for diamond single crystals shocked to 50–120 GPa in plate impact experiments. These results have provided the third-order elastic constants[27] and the elastic limit for shocked diamond.[26] Now that the shock response of cubic diamond is available[26,27] at stresses comparable to the end states measured in shocked HOPG,[18,19] a comprehensive and detailed analysis of the measured wave profiles is in order.

Here, we present numerical simulations of the wave profiles measured in HOPG shocked to 27–50 GPa (Ref. 19) to provide insight into the transformation time scales and into the nature of the high-pressure phase. Numerical simulations enable a detailed analysis of the measured wave profiles to incorporate the high-pressure phase response and to include wave reflections due to impedance mismatches at the shocked HOPG boundaries.

## II. COMPUTATIONAL METHODS

Our simulations used a multiphase material modeling approach in which the high-pressure phase of shocked HOPG was described using the recently reported nonlinear elastic response[27] of cubic diamond. Our modeling approach incorporated the usual separation[28] of the thermomechanical response into the mean stress response and the deviatoric stress response.

### A. Single-phase material description

The mean stress response for each phase was determined by constructing the Helmholtz potential[29] $F(T,V)$ from the isothermal compression curve at room temperature, the

 

TABLE I. Model parameters for graphite and cubic diamond phases.

| Parameter | Graphite Model | Diamond Model A | Diamond Model B |
|---|---|---|---|
| $V_0$ (cm$^3$/g) | 0.442 | 0.285 | 0.285 |
| $A$ (J/g K) | 0.561 | 0.193 | 0.193 |
| $B$ (J/g K) | 1.516 | 1.884 | 1.884 |
| $\theta_0$ (K) | 1715 | 1500 | 1500 |
| $\Gamma_0$ | 0.35 | 1.15 | 1.15 |
| $B_0$ (GPa) | 38.0 | 442 | 442 |
| $B'$ | 7.9 | 4.438 | 4.438 |
| $G_0$ (GPa) | 27 | 540 | 540 |
| $G_1$ | 0 | 4.156 | 4.156 |
| $G_2$ (GPa$^{-1}$) | 0 | −0.00553 | −0.00553 |
| $Y$ (GPa) | 1.0 | 0 | 49.0 |

specific heat at constant volume $c_v(T,V)$, and the Grüneisen parameter $\Gamma = \Gamma_0 V/V_0$. The isothermal compression curve was of the Murnaghan form,[30]

$$P(V) = \frac{B_0}{B'}\left[\left(\frac{V_0}{V}\right)^{B'} - 1\right], \tag{1}$$

where $V_0$ is the initial specific volume, $B_0$ is the isothermal bulk modulus at ambient pressure, and $B'$ is its pressure derivative. To provide a good match to published data for graphite and diamond, the specific heat was assumed to have the form

$$c_v(T,V) = A + B\frac{x^2 e^x}{(e^x-1)^2}, \tag{2}$$

where $A$ and $B$ are constants and $x = \theta(V)/T$. To provide thermodynamic consistency, we chose

$$\theta(V) = \theta_0 \exp\left[\frac{\Gamma}{V}(V_0 - V)\right]. \tag{3}$$

The deviatoric elastic response and the mechanical strength for each phase were described by the isentropic shear modulus $G$ and the yield stress $Y$, respectively. The shear modulus was determined using

$$G(P) = G_0 + G_1 P + G_2 P^2. \tag{4}$$

Due to a lack of information about the response of HOPG and the high-pressure phase to shock wave compression, the mechanical strength was described using the simplest physically reasonable model: We used a von Mises yield criterion[31] in which the yield stress $Y$, defined as the elastic limit under uniaxial stress loading conditions, was assumed to be constant.

Model parameters for each phase were determined by fitting available experimental data for graphite and cubic diamond and are listed in Table I. For the graphite phase, parameters for Eq. (1) were determined using available isothermal compression data,[32–35] together with the measured shock wave profiles.[19] For the specific heat, the constants $A$, $B$, and $\theta_0$ were determined by fitting the available heat capacity data[36] using Eqs. (2) and (3). The Grüneisen parameter at ambient pressure $\Gamma_0$ was taken from Ref. 37. Because the shock wave compression considered here was oriented approximately normal to the basal planes of the graphite lattice,[19] the shocked HOPG was assumed to possess significant strength (i.e., $Y \neq 0$). Also, the shear modulus was expected to be significant at high pressures due to increased interatomic interactions across the basal planes. Therefore, values for $Y$ and $G = G_0$ were chosen to provide a good match to the measured wave profiles.[19]

For the high-pressure phase, the mean stress and the deviatoric elastic responses were determined using the second- and third-order elastic constants of cubic diamond,[27] as described in the Appendix. The yield stress for the high-pressure phase was modeled using two bounding cases: For model A, a hydrodynamic response ($Y = 0$) was assumed. For model B, the yield stress was chosen to be sufficiently large to ensure that the deviatoric response (for the stress range of interest) was purely nonlinear elastic. To complete the thermomechanical description, the parameters $A$, $B$, and $\theta_0$ for the specific heat model were determined by fitting available experimental data[38] using Eqs. (2) and (3). The Grüneisen parameter $\Gamma_0$ for diamond was taken from Ref. 37.

### B. Multiphase modeling framework

The material models for the individual phases were incorporated into the multiphase modeling framework using appropriate mixture rules. For extensive variables, such as volume, the lever rule[29] gives

$$V = (1-\lambda_m)V_1 + \lambda_m V_2, \tag{5}$$

where $V_1$ and $V_2$ are the volumes of phases 1 and 2, respectively, and $\lambda_m$ is the mass fraction of phase 2. The shear modulus and yield stress of the mixture were determined using

$$\frac{1}{G} = \frac{(1-\lambda_V)}{G_1} + \frac{\lambda_V}{G_2} \tag{6}$$

and

$$Y = (1-\lambda_V)Y_1 + \lambda_V Y_2, \tag{7}$$

respectively, where $\lambda_V = \lambda_m V_2/V$ is the volume fraction of phase 2. Equation (6) is consistent with the assumption of stress equilibrium between the two phases.[39]

Because the shock-induced graphite-diamond transition occurs at stresses far from the equilibrium phase boundary[40] (defined by equality of the Gibbs free energies for the two phases), the transformation rate was determined using a stress criterion,

$$\begin{aligned} \dot{\lambda}_m &= C_1(\lambda_{\max} - \lambda_m) \quad P_x > P_{\rm tr} \\ \dot{\lambda}_m &= 0 \qquad\qquad\quad P_x < P_{\rm tr}, \end{aligned} \tag{8}$$

where $P_x$ is the longitudinal stress (positive in compression), $P_{\rm tr}$ is the transition threshold stress, and $C_1$ is a constant. To avoid numerical instabilities, the transformation rate was constrained to increase smoothly from zero by assuming

$$\lambda_{\max} = C_2[P_x - P_{\rm tr}], \tag{9}$$

where $\lambda_{\max} \leqslant 1$. The constant $C_2$ was chosen to ensure that the transformation proceeded to completion for all of the calculated wave profiles. $P_{\rm tr}$ was adjusted slightly to match

TABLE II. Parameters for multiphase model.

| Parameter | |
|---|---|
| $C_1$ ($s^{-1}$) | $5.0 \times 10^8$ |
| $C_2$ ($GPa^{-1}$) | 0.3 |
| $P_{tr}$ (GPa) | 19.0–21.5 |

each measured wave profile separately. Model parameters for the multiphase framework are listed in Table II.

### C. Calculation of wave profiles

The above multiphase modeling framework was incorporated into a one-dimensional wave propagation code[41] that solves the appropriate governing equations using the finite-difference, artificial viscosity approach.[28] Energy dissipation arising from the artificial viscosity was included in the calculations as entropy production, in keeping with the inherent irreversibility of shock wave compression. Also, work due to inelastic deformation is dissipated primarily as heat and was included as an additional source of entropy.

## III. RESULTS

Using the above material descriptions, the wave profiles reported in Ref. 19 were numerically simulated using the experimental configuration shown in Fig. 1, in which a copper plate impacted an HOPG sample backed by a LiF optical window. Also shown is the time-distance plot to indicate the propagating waves, including the reflection/transmission at the HOPG/LiF interface. For comparisons with published measurements,[19] simulations were performed for peak stresses of 27, 35, 41, and 50 GPa, and particle velocity profiles were

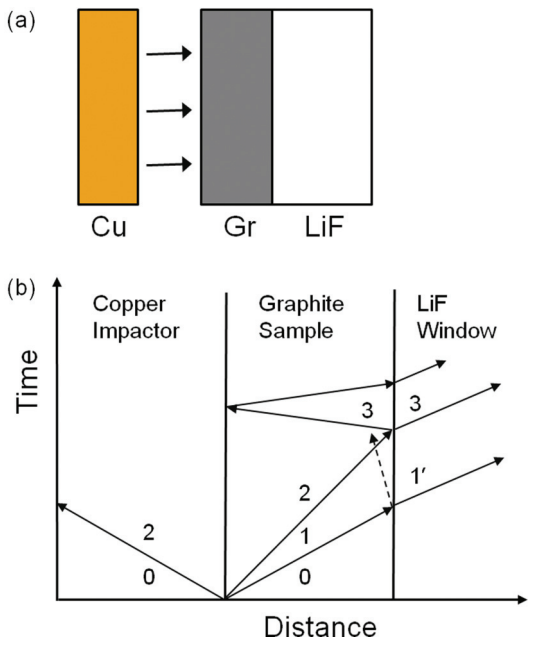


FIG. 1. (Color online) (a) Experimental configuration (Ref. 19) and (b) time versus distance diagram for wave propagation simulations. The numbers indicate end states for shock wave compression; 1′ and 3 correspond to the measured states.

calculated at the HOPG/LiF interface. In these calculations, copper and LiF were modeled using their known shock responses.[42]

Because wave propagation features in shocked HOPG were discussed previously,[19] only a brief summary is provided here. Upon impact, shock waves propagate from the impact surface into the HOPG sample and into the copper impactor (Fig. 1). For impact stresses larger than the transformation stress ($P_{tr}$), the shock wave in the HOPG splits into two waves due to the volume change associated with the transformation. The first wave brings the ambient HOPG to $P_{tr}$ (state 1 in Fig. 1) and the second wave brings the transformed HOPG to the high stress end state (state 2). The dashed arrow in Fig. 1 denotes a small, slow-moving reflected wave that results from the slight impedance mismatch at the HOPG/LiF interface. In contrast, the large volume change associated with the transformation wave results in a large compressive wave reflection at the HOPG/LiF interface that takes the transformed HOPG from state 2 to state 3. The experimentally measured profiles at the HOPG/LiF interface correspond to states 1′ and/or 3, depending on the peak stress.

As shown in Figs. 2(a)–2(c), a clean two-wave structure, with a transition stress of ~20 GPa, was experimentally observed[19] for HOPG shocked to 27, 35, and 41 GPa. For sufficiently large impact stresses, the transformation is overdriven (the second wave speed exceeds the first wave speed) and state 1 is not observed. Instead, a single wave takes the HOPG from the ambient state to the high-pressure phase or state 2 (state 3 in the measured profile) directly. The measured wave profile[19] for HOPG shocked to 50 GPa provides a case in point, as shown in Fig. 2(d). As noted above, states 1′ and 3 represent the states that are experimentally measured.

Comparisons of the calculated results with the measured wave profiles, shown in Fig. 2, reveal that the diamond model with no mechanical strength (model A) provides a poor match to the data. Significant differences are observed for both the second wave speed and the peak particle velocity. Thus, the high-pressure phase of shocked HOPG cannot be reconciled with a hydrodynamic material description of diamond.

In contrast, calculations performed using the nonlinear elastic model for diamond (model B) provide a good match to all the measured wave profiles, including the peak particle velocity, as shown in Fig. 2. The small feature appearing in the calculated wave profiles at later times is a wave reverberation in the high-pressure phase (see Fig. 1). The calculations show that the shocked HOPG is fully transformed within the rise time of the transformation wave (<10 ns). Therefore, because shock compression from state 2 to state 3 (Fig. 1) takes place in HOPG that is fully transformed, the measured peak particle velocity contains key information regarding the response of the high-pressure phase. Hence, the good match between our calculations using model B and the measured peak particle velocity provides important insight regarding the high-pressure phase, as discussed next by considering the shock end states.

## IV. ANALYSIS AND DISCUSSION

Stress, volume, and temperature states for all four wave profiles were determined from the calculations and are shown

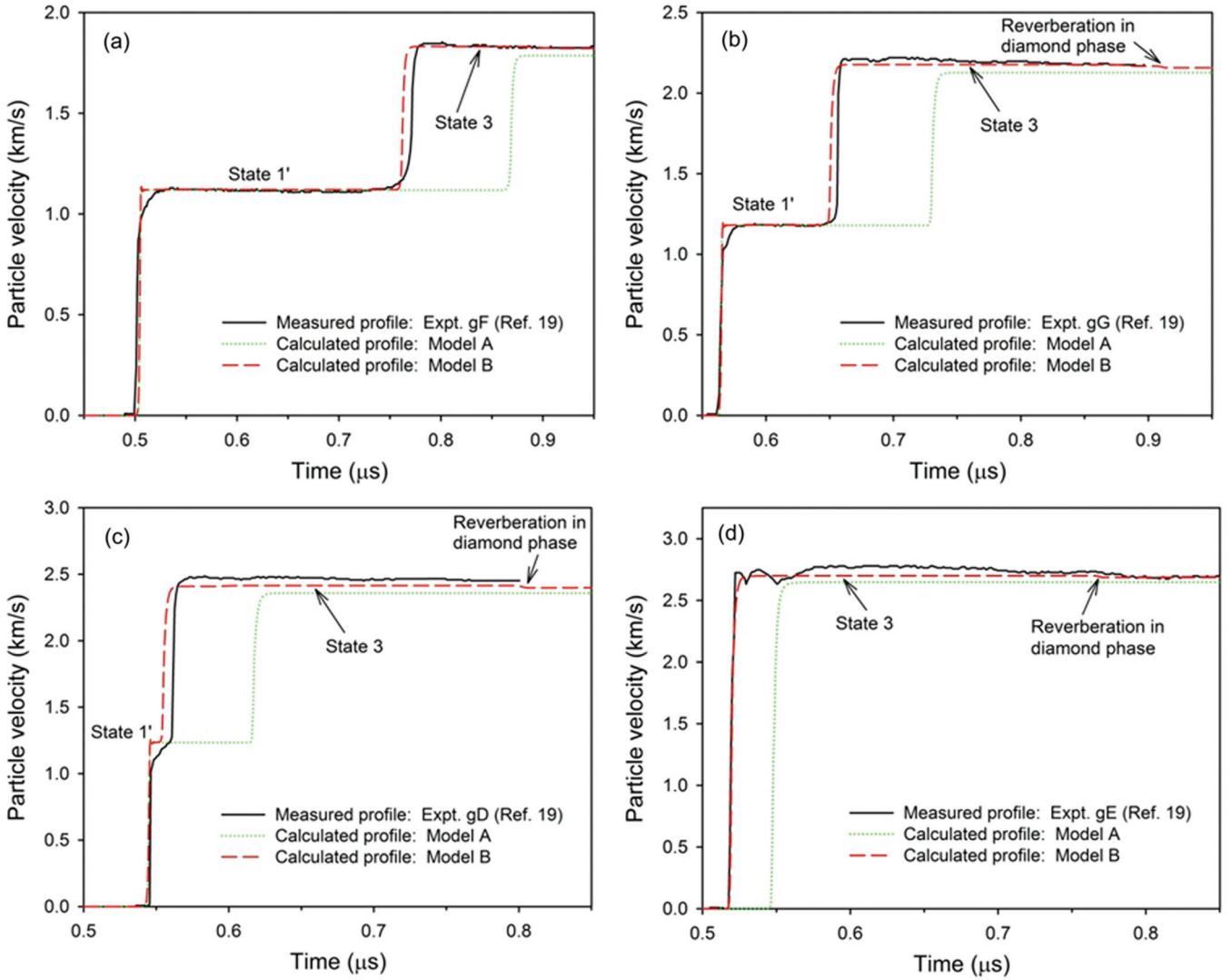


FIG. 2. (Color online) Particle velocity histories at the HOPG/LiF interface for peak stresses of (a) 27 GPa, (b) 35 GPa, (c) 41 GPa, and (d) 50 GPa. Measured histories are from Ref. 19. Model A: hydrodynamic diamond model (no mechanical strength). Model B: nonlinear elastic diamond model. Time is relative to the moment of impact.

in Table III. In Fig. 3, the calculated stresses and volumes for states 1 and 3 are compared with those determined experimentally.[19] For visual clarity, results for state 2 are not shown in the figure. The clean two-wave structure observed in the experiments enabled Erskine and Nellis to accurately determine the stress-volume states using well-established wave analysis methods.[19]

Below the transformation stress, stress-volume states calculated using models A and B agree well with each other and with the experimental results for state 1. This is expected because the same model for the graphite phase was used in both sets of calculations. Since no Hugoniot data have been published for HOPG shocked to stresses below the phase transition, the measured Hugoniot curve for partially oriented pyrolytic graphite[15] is shown for comparison. The good overall agreement observed for the low pressure phase suggests that, below 20 GPa, the shock response of various graphites is comparable. However, low stress data on shocked HOPG are needed to confirm this inference.

Above the transition, stress-volume states calculated using model A (hydrodynamic diamond model) do not match the experimental results[19] for shocked HOPG. However, they agree with the diamond Hugoniot[25] extrapolated from data at significantly higher stresses (>100 GPa).

In contrast, stresses and volumes calculated using model B (nonlinear elastic diamond response) demonstrate an excellent match to the experimental results[19] for states 2 (not shown) and 3, consistent with the wave profile results shown in Fig. 2. Furthermore, Fig. 3 shows that the calculated and the experimental stress-volume states, for the high-pressure phase, are in good agreement with the nonlinear elastic stress-volume curve for shock-compressed diamond. The elastic diamond curve was determined from the elastic constants provided in Ref. 27, using the procedure described in the Appendix.

The results in Fig. 3 provide an explanation for the differences reported previously[19] between the experimental stress-volume states for the high-pressure phase and the extrapolated diamond Hugoniot:[25] The extrapolated diamond Hugoniot

TABLE III. Calculated longitudinal (long.) stress, volume, and temperature for states 1–3 in shocked HOPG.

| Expt. No. (Reference 19) | Long. stress Model A (GPa) | Volume Model A ($cm^3/g$) | Temp. Model A (K) | Long. stress Model B (GPa) | Volume Model B ($cm^3/g$) | Temp. Model B (K) |
|---|---|---|---|---|---|---|
| *gF* (State 1) | 19.0 | 0.3625 | 600 | 19.0 | 0.3625 | 600 |
| *gG* (State 1) | 20.3 | 0.3600 | 620 | 20.3 | 0.3600 | 620 |
| *gD* (State 1) | 21.5 | 0.3577 | 645 | 21.5 | 0.3578 | 645 |
| *gE* (State 1) | N/A | N/A | N/A | N/A | N/A | N/A |
| *gF* (State 2) | 25.7 | 0.2725 | 1020 | 26.5 | 0.2856 | 900 |
| *gG* (State 2) | 33.4 | 0.2696 | 1260 | 34.7 | 0.2816 | 1170 |
| *gD* (State 2) | 39.5 | 0.2673 | 1440 | 41.2 | 0.2787 | 1380 |
| *gE* (State 2) | 47.8 | 0.2645 | 1700 | 49.8 | 0.2756 | 1760 |
| gF (State 3) | 35.8 | 0.2676 | 1040 | 36.7 | 0.2833 | 940 |
| *gG* (State 3) | 45.3 | 0.2642 | 1280 | 46.8 | 0.2790 | 1230 |
| *gD* (State 3) | 52.3 | 0.2619 | 1480 | 53.6 | 0.2762 | 1430 |
| *gE* (State 3) | 61.0 | 0.2592 | 1740 | 62.7 | 0.2731 | 1810 |

constitutes the hydrodynamic diamond response, whereas the experimental stress-volume states (and the measured wave profiles in Fig. 2) are consistent with the nonlinear elastic diamond response. Hence, the previous suggestion[19] that shocked HOPG transforms to a diamondlike phase having a density 5% less than diamond is neither needed nor supported by our calculations. Instead, our calculations demonstrate that the stiffness and density of the high-pressure phase of shocked HOPG are entirely consistent with the experimentally determined[26,27] elastic response of shock-compressed cubic diamond.

The present results show that shocked HOPG transforms to diamond in less than 10 ns and the mechanical response of the diamond formed on this time scale is nonlinear elastic. The rapid transformation in shocked HOPG is in contrast to the longer time scales expected for the proposed reconstructive transformation mechanisms associated with shocked graphite powders.[16,43]

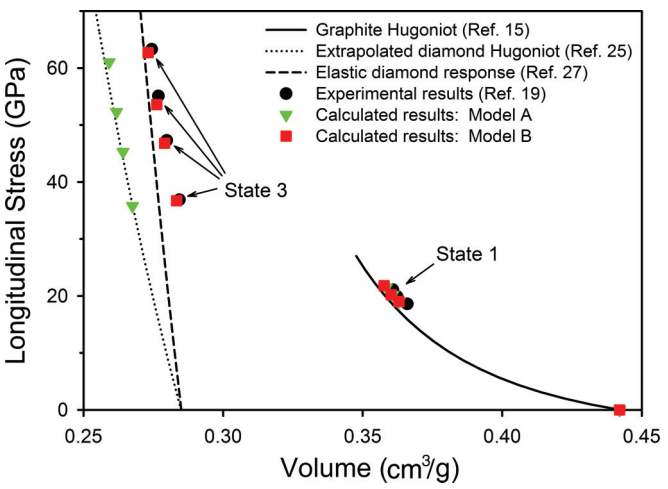


FIG. 3. (Color online) Stress-volume end states for shocked HOPG. The black circles are end states determined from the measured wave profiles (Ref. 19). The green triangles are end states calculated using model A (hydrodynamic diamond model). The red squares are end states calculated using model B (nonlinear elastic diamond model). States 1 and 3 are defined in Fig. 1. The solid curve is the measured Hugoniot for pyrolytic graphite (not HOPG) (Ref. 15). The dotted curve is the diamond Hugoniot extrapolated from higher stresses (>100 GPa) (Ref. 25). The dashed curve is the longitudinal elastic response of diamond, determined using the second- and third-order elastic constants (Ref. 27) (see Appendix).

## V. CONCLUSIONS

A rigorous analysis of the measured plane wave profiles[19] for HOPG shocked to 27–50 GPa has led to important insight into the shock-induced graphite to diamond transformation. Using a multiphase material model for HOPG/diamond that incorporates mechanical strength, our numerical simulations show that shocked HOPG transforms to a high-pressure phase having stiffness and density that are consistent with cubic diamond, in contrast to previous suggestions.[19] Additionally, our calculations show that the diamond phase formed responds as a nonlinear elastic solid, consistent with recent experimental results for shocked diamond single crystals.[26,27]

The work described here has addressed long-standing scientific questions regarding the real-time formation and mechanical response of the diamond phase in the shock-induced graphite to diamond transformation. However, our findings have also raised new and interesting questions: Are the findings reported here unique to HOPG, and what are the precise atomistic mechanisms that result in the HOPG-to-diamond transformation on such short time scales? Answers to these questions will require well-characterized shock wave experiments on graphite samples having different microstructures and polycrystalline textures. Regarding microscopic mechanisms, wave profile measurements and analyses reported here will need to be augmented with real-time x-ray diffraction measurements[44,45] and related analyses in shock-compression experiments. Such developments are now underway.

## ACKNOWLEDGMENTS

We acknowledge Dr. J. N. Johnson for useful discussions regarding the multiphase equation of state. This work was supported by the Department of Energy through Grants No. DE-FG03-97SF21388 and No. DE-NA0000970.


## APPENDIX: ELASTIC RESPONSE OF HIGH-PRESSURE PHASE OF SHOCKED HOPG

Model parameters describing the mean stress response and the deviatoric elastic response of polycrystalline cubic diamond were determined from the measured second-order[46] and third-order[27] isentropic elastic constants using the following orientational averaging procedure. The Cauchy stresses $\sigma_i'$ for uniaxial elastic strain along an arbitrary crystal direction were determined using

$$\sigma_1' = \frac{\rho_0}{\rho}\left[C_{11}'\eta_1' + \frac{1}{2}C_{111}'\eta_1'^2\right], \tag{A1}$$

$$\sigma_2' = \frac{\rho}{\rho_0}\left[C_{12}'\eta_1' + \frac{1}{2}C_{112}'\eta_1'^2\right], \tag{A2}$$

$$\sigma_3' = \frac{\rho}{\rho_0}\left[C_{13}'\eta_1' + \frac{1}{2}C_{113}'\eta_1'^2\right], \tag{A3}$$

where $\rho_0$ is the initial density, $\rho$ is the density in the strained state, $C_{ij}'$ and $C_{ijk}'$ are the second- and third-order elastic constants, and $\eta_1' = [(\rho_0/\rho)^2 - 1]/2$ is the uniaxial Lagrangian strain. In Eqs. (A1)–(A3), the contracted Voigt notation[47] has been used for the tensor indices and the primes indicate that the tensor components are expressed in a coordinate system aligned along the direction of uniaxial strain. Equations (A1)–(A3) were evaluated for uniaxial strains along a set of directions that provided a sampling of all possible crystal orientations. The stress components determined from these calculations were averaged over all crystal directions to obtain stress-density curves for the longitudinal and lateral stresses. The mean stress curve was determined using $\sigma_m = (\sigma_1 + \sigma_2 + \sigma_3)/3$, where $\sigma_i$ are the orientationally averaged stress components.

Strictly speaking, the above stress-density relationships are isentropic loading curves. However, differences between isentropic and isothermal loading conditions are negligible for elastic compression of diamond to stresses less than 100 GPa. Therefore, $B_0$ and $B'$ for diamond were determined by fitting the averaged mean stress curve using Eq. (1).

The shear modulus $G(P)$ was determined using the averaged longitudinal and mean stress curves determined above, together with the relationship[31]

$$G = \tfrac{3}{4}(L - B), \tag{A4}$$

where $L$ is the longitudinal elastic modulus. Shear modulus results determined using Eq. (A4) were fit using Eq. (4).


[1] P. S. DeCarli and J. C. Jamieson, Science **133**, 1821 (1961).
[2] G. E. Duvall and R. A. Graham, Rev. Mod. Phys. **49**, 523 (1977).
[3] R. E. Hanneman, H. M. Strong, and F. P. Bundy, Science **155**, 995 (1967).
[4] R. S. Clarke, Jr., D. E. Appleman, and D. R. Ross, Nature **291**, 396 (1981).
[5] P. S. DeCarli, US Patent No. 3238019 (1966).
[6] G. R. Cowan, B. W. Dunnington, and A. H. Holtzman, US Patent No. 3401019 (1968).
[7] F. P. Bundy, W. A. Bassett, M. A. Weathers, R. J. Hemley, H. K. Mao, and A. F. Goncharov, Carbon **34**, 141 (1996).
[8] B. J. Alder and R. H. Christian, Phys. Rev. Lett. **7**, 367 (1961).
[9] M. N. Pavlovskii and V. P. Drakin, JETP Lett. **4**, 116 (1966).
[10] R. G. McQueen and S. P. Marsh, in *Behavior of Dense Media under High Dynamic Pressure* (Gordon and Breach, New York, 1968), p. 207.
[11] L. F. Trueb, J. Appl. Phys. **39**, 4707 (1968).
[12] L. F. Trueb, J. Appl. Phys. **42**, 503 (1971).
[13] P. S. DeCarli, in *Proceedings of the Sixth AIRAPT Conference: High Pressure Science and Technology*, edited by K. D. Timmerhaus and M. S. Barber (Plenum, New York, 1979), Vol. 1, p. 940.
[14] D. G. Morris, J. Appl. Phys. **51**, 2059 (1980).
[15] W. H. Gust, Phys. Rev. B **22**, 4744 (1980).
[16] P. S. DeCarli, in *Mechanical Behavior of Diamond and Other Forms of Carbon*, edited by M. D. Drory, D. B. Bogy, M. S. Donley, and J. E. Field, Materials Research Society Symposium Proceedings Vol. 383 (Materials Research Society, Pittsburgh, 1995), p. 21.
[17] S. V. Pyaternev, S. V. Pershin, and A. N. Dremin, Combust., Expl. Shock Waves **22**, 756 (1986).
[18] D. J. Erskine and W. J. Nellis, Nature **349**, 317 (1991).
[19] D. J. Erskine and W. J. Nellis, J. Appl. Phys. **71**, 4882 (1992).
[20] E. Vlodarchik and R. Trebinski, Shock Waves **7**, 231 (1997).
[21] R. Abeyaratne and J. K. Knowles, J. Appl. Phys. **87**, 1123 (2000).
[22] O. Bruno and D. Vaynblat, Proc. R. Soc. London, Ser. A **457**, 2871 (2001).
[23] W. Wang, M. S. Hall, K. S. Moe, J. Tower, and T. M. Moses, Gems Gemol. **43**, 294 (2007).
[24] W. Wang and T. M. Moses, Gems Gemol. **47**, 227 (2011).
[25] M. N. Pavlovskii, Sov. Phys. Solid State **13**, 741 (1971).
[26] J. M. Lang, Jr. and Y. M. Gupta, J. Appl. Phys. **107**, 113538 (2010).
[27] J. M. Lang, Jr. and Y. M. Gupta, Phys. Rev. Lett. **106**, 125502 (2011).
[28] M. L. Wilkins, in *Methods in Computational Physics*, edited by B. Alder, S. Fernbach, and M. Rotenberg (Academic Press, New York, 1964), Vol. 3, p. 211.
[29] H. B. Callen, *Thermodynamics and an Introduction to Thermostatistics*, 2nd ed. (Wiley, New York, 1985).
[30] F. D. Murnaghan, *Finite Deformation of an Elastic Solid* (Wiley, New York, 1951).
[31] See, for example, L. E. Malvern, *Introduction to the Mechanics of a Continuous Medium* (Prentice-Hall, Englewood Cliffs, NJ, 1969), p. 337.
[32] R. W. Lynch and H. G. Drickamer, J. Chem. Phys. **44**, 181 (1966).
[33] M. Hanfland, H. Beister, and K. Syassen, Phys. Rev. B **39**, 12598 (1989).

[34] Y. X. Zhao and I. L. Spain, Phys. Rev. B **40**, 993 (1989).
[35] T. Yagi, W. Utsumi, M. A. Yamakata, T. Kikegawa, and O. Shimomura, Phys. Rev. B **46**, 6031 (1992).
[36] W. C. Morgan, Carbon **10**, 73 (1972).
[37] M. van Thiel and F. H. Ree, Int. J. Thermophys. **10**, 227 (1989).
[38] A. C. Victor, J. Chem. Phys. **36**, 1903 (1962).
[39] R. Hill, J. Mech. Phys. Solids **11**, 357 (1963).
[40] F. D. Rossini and R. S. Jessup, J. Res. Natl. Bur. Stand., Sect. C **21**, 491 (1938).
[41] Y. M. Gupta, *COPS Wave Propagation Code* (SRI International, Menlo Park, CA, 1976).
[42] *LASL Shock Hugoniot Data*, edited by S. P. Marsh (University of California Press, Los Angeles, 1980).
[43] M. J. Buerger, in *Phase Transformations in Solids*, edited by R. Smoluchowski, J. E. Mayer, and W. A. Weyl (Wiley, New York, 1951), p. 183.
[44] S. J. Turneaure and Y. M. Gupta, J. Appl. Phys. **105**, 053520 (2009).
[45] S. J. Turneaure and Y. M. Gupta, J. Appl. Phys. **106**, 033513 (2009).
[46] H. J. McSkimin and P. Andreatch, Jr., J. Appl. Phys. **43**, 2944 (1972).
[47] K. Brugger, Phys. Rev. **133**, A1611 (1964).